A Letters Journal Exploring the Frontiers of Physics

May 2017

EPL, **118** (2017) 38003 www.epljournal.org
doi: 10.1209/0295-5075/118/38003

Chaos-free oscillations

Joana G. Freire[1,2(a)], Marcia R. Gallas[1,2,3] and Jason A. C. Gallas[1,2,3]

[1] *Complexity Sciences Center - 9225 Collins Avenue #1208, Surfside, FL 33154, USA*
[2] *Departamento de Física, Universidade Federal da Paraíba - 58051-970 João Pessoa, Brazil*
[3] *Max-Planck-Institut für Physik komplexer Systeme - Nöthnitzer Str. 38, D-01187 Dresden, Germany*

received 12 May 2017; accepted in final form 14 June 2017
published online 7 July 2017

PACS 82.40.Bj – Chemical kinetics and reactions: special regimes and techniques: Oscillations, chaos, and bifurcations
PACS 89.75.Fb – Structures and organization in complex systems
PACS 05.45.Pq – Numerical simulations of chaotic systems

Abstract – Oscillators have widespread applications in micro- and nanomechanical devices, in lasers of various types, in chemical and biochemical models, among others. However, applications are normally marred by the presence of chaos, requiring expensive control techniques to bypass it. Here, we show that the low-frequency limit of driven systems, a poorly explored region, is a wide chaos-free zone. Specifically, for a popular model of micro- and nanomechanical devices and for the Brusselator, we report the discovery of an unexpectedly wide mosaic of phases resulting from stable periodic oscillations of increasing complexity but totally free from chaos.

Introduction. – The general subject of forced vibrations was discussed rather fully by different authors in recent years, motivated by novel practical applications, most notably involving micro- and nanomechanical devices [1–8]. Currently, a significant part of the literature deals with problems of chaos synchronization and chaos control, this latter topic being even considered now a young discipline expanding the scope of traditional research fields in physics and engineering.

Chaos is characterized by sensitive dependence on the initial conditions, such that minute perturbations may lead to substantial changes in the global dynamics, in particular to the stabilization of chaos into periodic orbits. Nowadays, different techniques to control chaos are in use. For instance, in the so-called feedback methods [9,10] a suitably selected perturbation is applied to a system, thereby inducing the stabilization of some unstable periodic orbit. In contrast, non-feedback control methods involve applying small harmonic perturbations to induce stabilization [11]. Chaos and regularity seem to be two intrinsically connected phenomena sharing, in usually rather complicated "fractal" ways, the control parameter space of physical systems. Although some applications may benefit from chaos, *e.g.*, in data encryption, the majority of others is marred by chaos and by the need for expensive control techniques to bypass it.

Our objective is quite different. We report the discovery of wide chaos-free regions in the control parameter space which, nevertheless, support a large quantity of intrinsically stable complex oscillations *ab ovo*. Specifically, we show that the low-frequency limit of driven systems, a poorly explored domain, puts *large chaos-free regions* at our disposal. In addition, the low-frequency limit also displays *systematic accumulations of periodic oscillations* whose waveforms have a number of spikes that seem to grow without bound as a function of control parameters.

As working example we consider the prototypical Duffing oscillator [12–14]. This choice is motivated by its ever increasing use in nanoscale systems, to describe properties of micro- and nanomechanical devices [1–8]. In spite of the attention that this oscillator has drawn in recent years, several aspects remain poorly understood. We find the low-frequency limit of the Duffing oscillator to display unexpectedly regular mosaics in the control parameter space, corresponding to stable periodic oscillations of increasingly complex waveforms. Although we focus here on the Duffing oscillator, similar chaos-free zones were also found in other driven systems and will be discussed elsewhere [15].

Model and simulations. – Since the seminal observations of chaos, the Duffing oscillator played a key role in nonlinear dynamics [12–14]. As is known, a Duffing-like oscillator was the first system were chaos was observed

(a) Present address: Instituto Dom Luiz, Faculdade de Ciências, Universidade de Lisboa - 1749-016 Lisbon, Portugal.

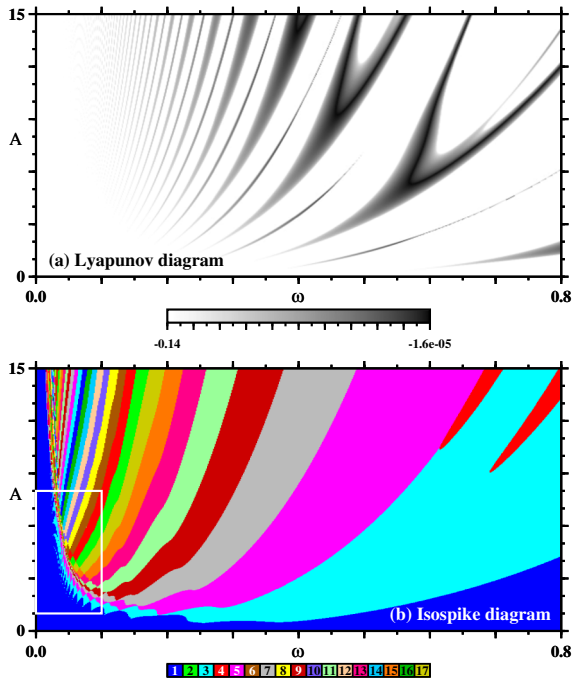

Fig. 1: (Color online) Two complementary characterizations of stability: (a) standard Lyapunov stability diagram; (b) stability diagram displaying with colors the number of spikes per period, isospikes [21,22] in oscillations of x. The Lyapunov diagram (a) does not reveal the waveform complexifications shown by the isospike diagrams. Note the absence of chaos in these panels. The white box in (b) is shown magnified in fig. 2(a).

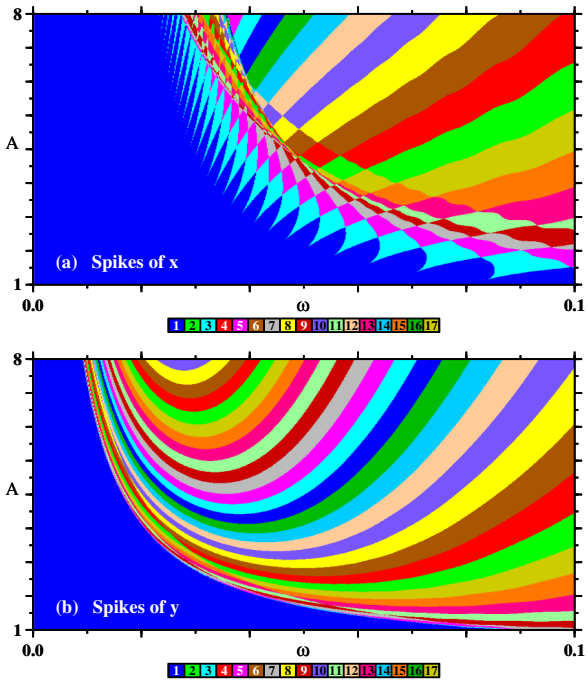

Fig. 2: (Color online) Details of the chaos-free stability mosaics. (a) Magnification of the white box in fig. 1(b) showing the distribution of spikes in the x variables of eq. (1). (b) Corresponding mosaic for the y variable.

experimentally, by Ueda [16] in 1960–1961. Recently, Duffing-like proxies have been found to present the distinctive technological advantage of bypassing noisy spectra which normally pollute driven (*i.e.*, non-autonomous) oscillators [17]. An additional characteristic is that such oscillator is among the most precise devices presently in existence, allowing its oscillation modes to be measured with very high accuracy. A quantum Duffing oscillator has been proposed for the efficient and reliable detection of a quantum-mechanical state of nanoscale systems, qubit state detection, in the present designs of quantum circuits [18].

We consider Duffing's equation written as usual as

$$\dot{x} = y, \qquad \dot{y} = \alpha x - \beta x^3 - \delta y + A\cos(\omega t), \qquad (1)$$

where α and β define the nature of the oscillator, δ controls the dissipation, and A and ω are the amplitude and angular frequency of the external drive, respectively. We use the standard values from the literature [12,19,20] $(\alpha, \beta, \delta) = (-1, 1, 0.2)$.

The stability diagrams shown in figs. 1–3 were obtained by dividing the parameter windows shown into a 600×600 mesh of equally spaced points and computing three quantities for every point of the mesh: i) the Lyapunov spectrum and, for the periodic oscillations, we computed also ii) their period and iii) the number of spikes per period of x and y. To this end, eq. (1) was integrated numerically using the standard fourth-order Runge-Kutta algorithm with fixed time-step $h = 0.01$. Integrations started at $t = 0$ always from the same arbitrary initial condition, $(x, y) = (0, 0)$. The first 0.3×10^6 integration steps were discarded as a transient needed to approach the attractor. The subsequent 6×10^6 time steps were used to determine the Lyapunov spectrum. After computing the Lyapunov spectrum, integrations were continued for an additional 3×10^6 time steps, when we recorded up to 1600 extrema (maxima and minima) of x and y together with the instant when they occur. This record allowed obtaining the period for each parameter point, as well as the number of spikes within a period of x and y.

The chaos-free mosaics. – Figures 1 and 2 show stability diagrams for the Duffing oscillator, in the frequency ω *vs.* the amplitude A of the external drive. Figure 1(a) shows a familiar Lyapunov stability diagram, while fig. 1(b) shows a diagram displaying in colors parameter regions characterized by periodic oscillations having the same number of spikes per period in the variable x, as indicated by the colorbar under the diagram. This type of diagram is called *isospike diagram* [21,22] and its colors allow one to quickly grasp how the number of spikes varies as control parameters are tuned. In the limit $\omega \to 0$, the isospike diagram shows a conspicuous symmetrical accumulation of oscillations with an ever-increasing number of spikes, something not recognizable from the Lyapunov diagram. Note the conspicuous absence of chaos in these windows.

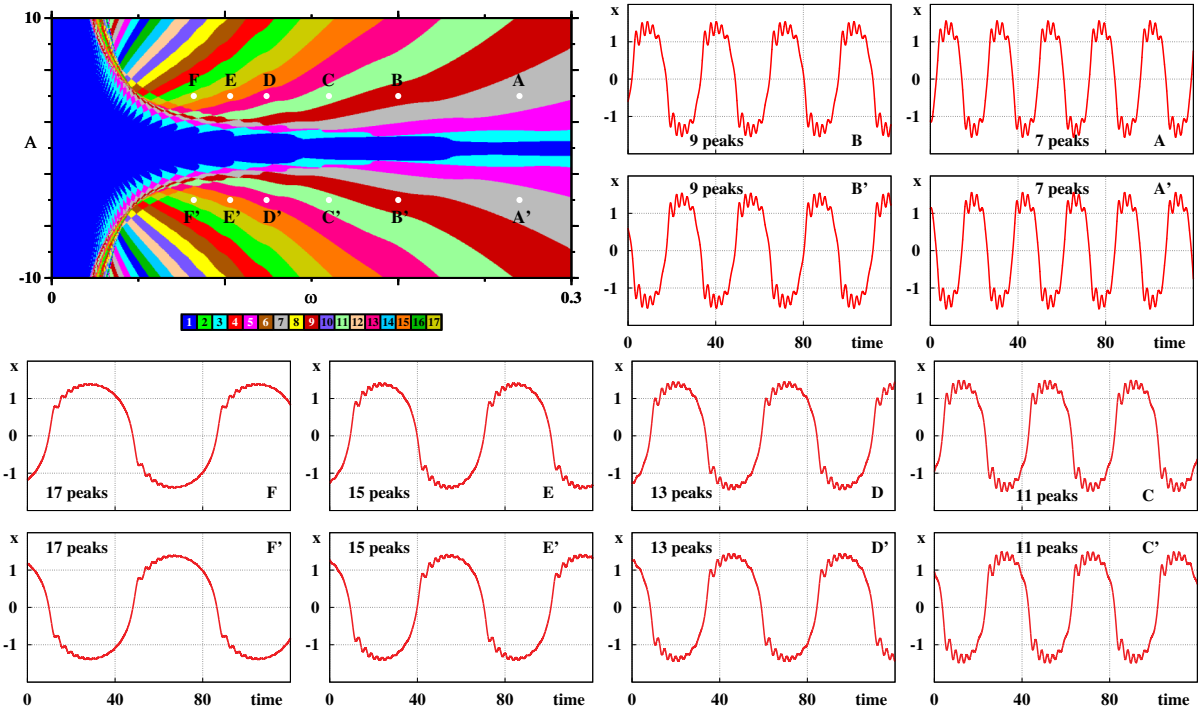

Fig. 3: (Color online) Systematic waveform complexification of the x oscillations. The oscillation amplitude decreases with the frequency in the accumulation limit $\omega \to 0$, while the period and the number of spikes per period grow. Note the absence of chaos, the $T/2$ shift between primed and unprimed signals, and that oscillations are antiperiodic [23–27], *i.e.*, they obey eq. (2). See text.

We use a palette of 17 colors to represent the number of spikes (local maxima) per period. The number 17 is chosen arbitrarily and changing it does not alter the distribution of spikes, just the sequence of colors in the diagrams. Patterns with more than 17 spikes per period are plotted by recycling the 17 colors "modulo 17": Multiples $17 \times \ell$ of 17 are plotted with the color index corresponding to $(18 - \ell)$ mod 17, namely $34 \equiv 16$ for $\ell = 2$, $51 \equiv 15$ for $\ell = 3$, $68 \equiv 14$ for $\ell = 4$, etc. Thus, our algorithm is designed to carefully detect periodicity. Black is used to represent the lack of numerically detected periodicity. If present, chaos and quasiperiodicity would be represented in black. In all the diagrams here, no black windows are present, not a single black pixel was recorded. Divergent solutions are characterized with a distinctive shading but do not occur in the present diagrams either.

The computation of stability diagrams classifying complex oscillations is a numerically demanding task, done here with in-house FORTRAN software developed to generate each figure directly as Postscript bitmap output with special compressed encoding, designed to reduce the size of the resulting files, and to maximize color contrast. Such computations were described in detail previously, *e.g.*, in refs. [17,22], where efficient methods to deal both with numerical and experimental data are given. Note that isospike diagrams require considerably less computations than Lyapunov diagrams and provide direct and useful complementary informations.

Figure 2 illustrates the regular tiling induced in the control parameter space by the self-organization of a rich variety of multipeaked periodic oscillations of the x and y variables in the $\omega \to 0$ limit. As is obvious from fig. 2, both mosaics depend strongly on the variable used to count the spikes. When moving from the right to the left on the panels, the number of spikes per period grows very fast towards $\omega = 0$. An important feature in fig. 2 is the total absence of chaotic phases. The blue stripe on the left-hand side of fig. 2 shows that there is a considerable interval of small values of ω where the number of spikes remains equal to one per period, meaning a *no-impact* ω *window*. In other words, there is a certain *threshold value* of ω beyond which there is an effective impact on the dynamics, *i.e.*, topological changes occur in phase-space trajectories.

Waveform complexification. – The leftmost panels in the top row of figs. 3 and 4 display a number of representative points of the mosaics, indicated by white dots and by primed and unprimed letters. The figures show how the waveforms of x and y get more and more spikes added to them as ω decreases and, more importantly, that the waveforms of x and y suffer rather distinct changes in form and amplitude. Such waveforms were obtained by integration of eq. (1) from the arbitrary initial condition $(x, y) = (0, 0)$. In figs. 3 and 4, dots are located symmetrically along the lines $A = 4$ and $A = -4$. Their coordinates, period and number of spikes corresponding to the waveforms displayed in figs. 3 and 4 are listed in table 1. Note that, although numbers in this table obey the relation $\omega = 2\pi/T$, the V-shaped and rounded regions

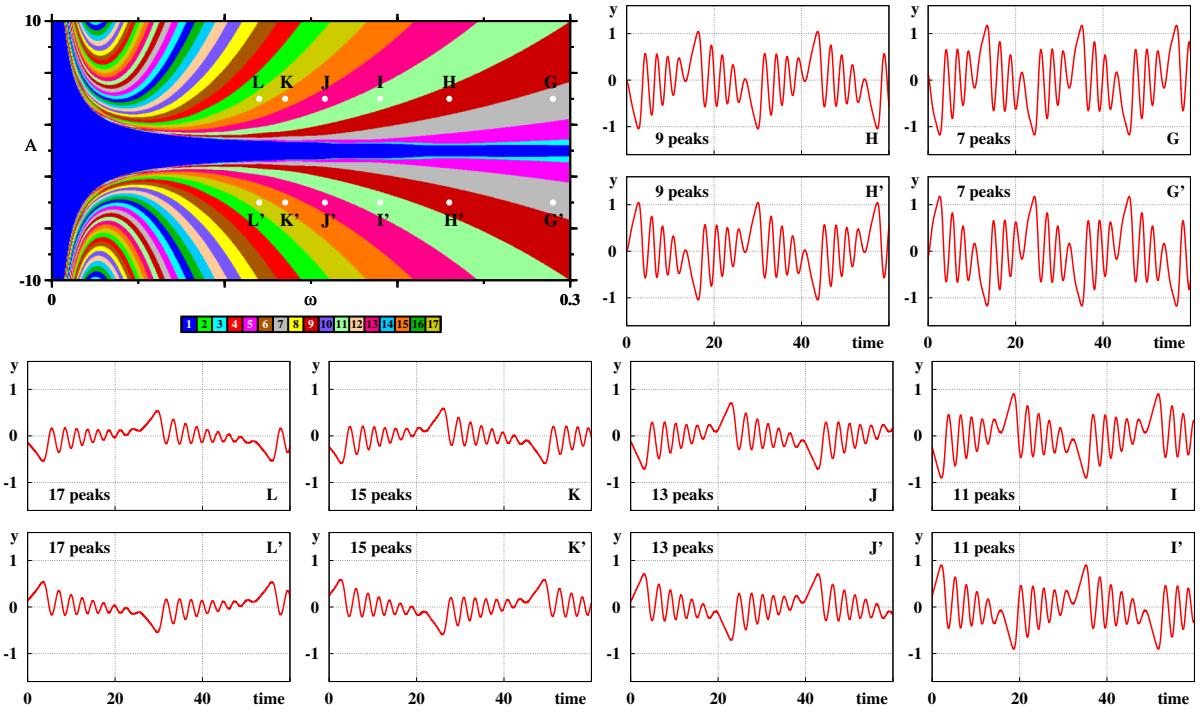

Fig. 4: (Color online) Same as in fig. 3, but for y oscillations, which display more pronounced amplitude variations.

seen in fig. 2 do not touch down rational numbers as in resonance tongues or mode locking.

Figures 3 and 4 show the waveform complexification observed when moving across the distinct phases composing the mosaic. The waveforms are representatives of the waveforms found inside the regions where the dot is located. In both figures, the sequence of waveforms reveals an unexpectedly regular and rather symmetrical evolutions. Remarkably, the evolutions are *antiperiodic oscillations*, a name already used in the 1950s [23–27]. Antiperiodic oscillations are a special type of periodic oscillations which obey the relation

$$s(t + T/2) = -s(t), \tag{2}$$

where the *signal* $s(t)$ represents either $x(t)$ or $y(t)$ and T denotes the period of the signal. The mosaic reflects the symmetry $(X, Y, A) \mapsto (-X, -Y, -A)$ of the equations of motion, eq. (1), as well as the shift symmetry underlying the trigonometric drive, namely the fact that $\cos(\omega t+\pi) = -\cos(\omega t)$, responsible for the $T/2$ shift [13,16]. Despite the intense scrutiny of the Duffing oscillator, as far as we know the implications of such combined symmetries for stability diagrams have not been appreciated yet.

Figures 3 and 4 allow one to grasp the nature of the spike-adding mechanism responsible for the regular tiling observed at low frequencies. Oscillations are characterized by two distinct time scales which may be easily discriminated by a simple Fourier analysis: superimposed to a slowly varying component there are fast oscillations forming sequences of small spikes. In the low-frequency limit, the relatively slowly varying oscillations acquire localized trains of spikes that get more and more spikes whose amplitude gets smaller and smaller. By suitably tuning the step of integration and initial conditions, we found no difficulties to detect an ever increasing number of spikes with tiny differences in their amplitudes. In other words, numerical experiments show that the scenario described is robust. We see no reason to expect departures from the scenario described for the self-organization of the low-frequency limit.

Table 1: Coordinates and number of spikes of the points marked in figs. 3 and 4 for $A = 4$. The symmetrical points at $A = -4$ have the same period and the same number of spikes, as indicated by the colors in figures.

	A	B	C	D	E	F
ω	0.27	0.2	0.16	0.124	0.103	0.082
T	23.27	31.41	39.27	50.68	61	76.62
p_x	7	9	11	13	15	17
	G	H	I	J	K	L
ω	0.29	0.23	0.19	0.158	0.135	0.12
T	21.66	27.32	33.07	39.77	46.54	52.35
p_y	7	9	11	13	15	17

As a second example of a wide chaos-free region, fig. 5 shows the low-frequency region for the well-known driven Brusselator [28–34] defined by the equations

$$\frac{\mathrm{d}X}{\mathrm{d}t} = A - (B+1)X + YX^2 + a\cos(\omega t), \tag{3}$$

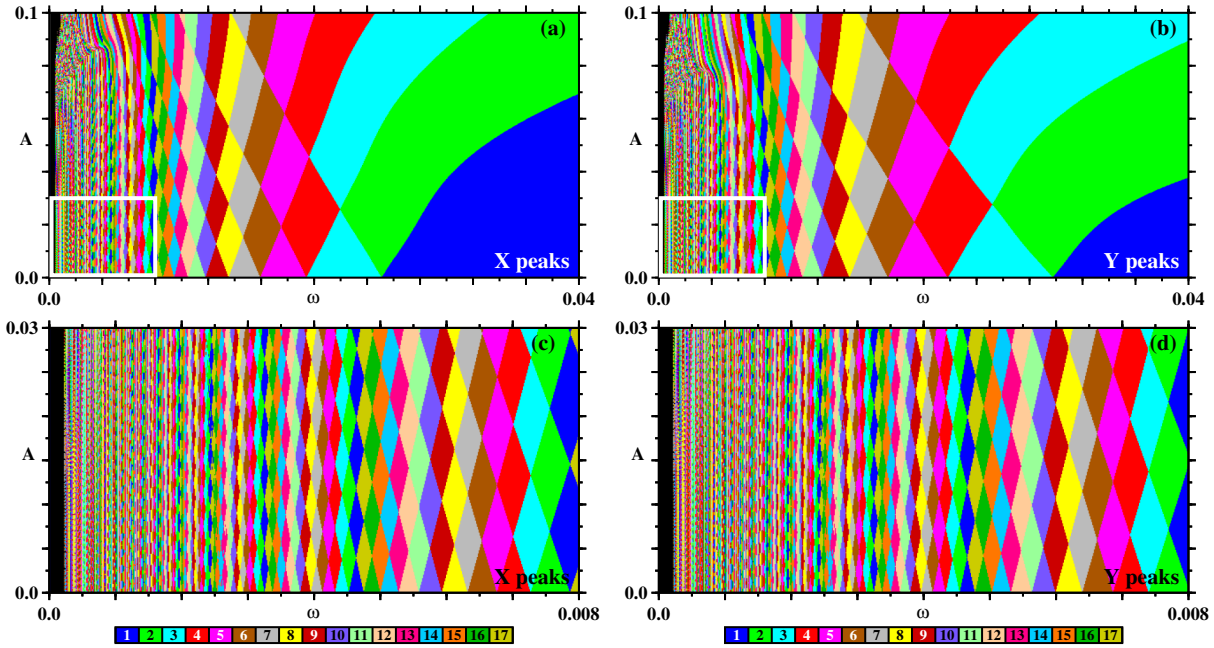

Fig. 5: (Color online) Chaos-free mosaics in the low-frequency domain observed by counting spikes per period of the oscillations of a driven Brusselator, defined by eqs. (3) and (4). (a) Counting spikes in X, and (b) counting spikes of Y. White boxes in (a) and (b) are shown magnified in panels (c) and (d), respectively. Here $(a, B) = (0.4, 1.2)$.

$$\frac{\mathrm{d}Y}{\mathrm{d}t} = BX - YX^2. \tag{4}$$

In the equations above we keep the standard naming of the parameters as used in the literature because there is now the risk of confusing them with those used in eq. (1). Figure 5 shows that the driven Brusselator also displays the same organization as discussed above for the Duffing oscillator. In fig. 5, black represents a region where the fixed integration step of the Runge-Kutta integrator becomes too big to correctly detect the rapidly increasing number of spikes in the oscillations. By decreasing the integration step one can eliminate part of the black stripe until the integration step becomes too big again, needing to be further reduced, and so on. Such reductions make computations very time-consuming but seem to add nothing essential to the diagram. In other words, the number of spikes seems to increase continuously without bound when $\omega \to 0$. For additional details and examples see ref. [15].

Conclusions and outlook. – This paper studied the behavior of two paradigmatic oscillators subjected to a low-frequency external periodic drive. Of interest was to investigate the global self-organization of stability phases resulting from *periodic motions* with an arbitrarily large number of spikes per period. Surprisingly, the low-frequency limit was found to display wide regions of complex and stable oscillations where chaos is totally absent. Such oscillations form *cascades of stability phases* which display intricate accumulations, which remain to be investigated. The low-frequency oscillations evolve in fast and slow time scales and unfold following non-chaos–mediated mixed-mode patterns. Such variations as well as their antiperiodic nature should not be difficult to observe in laboratory experiments.

In 1992, Lorenz insightfully remarked that "Now that computers have become ubiquitous, carefully conceived numerical experiments can enable us to explore a fascinating mathematical world that has not yet opened its doors to classical analytical procedures" [35]. The unexpected self-organization of oscillations and chaos-free stability regimes found in the low-frequency limit of well-studied oscillators seem to witness the foresight power of numerical experiments in regions which are still totally out of reach for analytical methods. A perplexing feature of the low-frequency region is that, contrary to what might have been expected, the V-shaped and rounded regions seen in our figures do not touch down rational numbers as in familiar phenomena normally found at high frequencies, namely resonance horns, tongues or mode locking. Since in the chaos-free regime the frequency is a natural small parameter, maybe it could be possible now to establish analytically the critical boundaries for the onset of the aforementioned phenomena familiar from the high-frequency region. This remains to be accomplished.

* * *

JGF was supported by a FCT postdoctoral fellowship (SFRH/BPD/101760/2014), Portugal. JACG was supported by CNPq, Brazil. This work was supported by the Max-Planck Institute for the Physics of Complex Systems, Dresden, in the framework of the Advanced Study Group on Optical Rare Events.

REFERENCES

[1] Braun D. J., *Phys. Rev. Lett.*, **116** (2016) 044102.
[2] Mahboob I. *et al.*, *Nano Lett.*, **15** (2015) 2312.
[3] Abdi M. *et al.*, *Phys. Rev. Lett.*, **114** (2015) 173602.
[4] Matheny M. H. *et al.*, *Phys. Rev. Lett.*, **112** (2014) 014101.
[5] Weber P. *et al.*, *Nano Lett.*, **14** (2014) 2854.
[6] Agrawal D. K., Woodhouse J. and Seshia A. A., *Phys. Rev. Lett.*, **111** (2013) 084101.
[7] Elishakoff I. (Editor), *Mechanical Vibration: Where do We Stand?* (Springer, Wien) 2007.
[8] Cleland A. N., *Foundations of Nanomechanics, From Solid-State to Device Applications* (Springer, Berlin) 2003.
[9] Scholl E. and Schuster H. G. (Editors), *Handbook of Chaos Control*, 2nd edition (Wiley-VHC, Weinheim) 2007.
[10] Chen G. and Yu X. (Editors), *Chaos Control, Theory and Application* (Springer, Berlin) 2003.
[11] Meucci R., Euzzor S., Pugliese E., Zambrano S., Gallas M. R. and Gallas J. A. C., *Phys. Rev. Lett.*, **116** (2016) 044101.
[12] Kovacic I. and Brennan M. J. (Editors), *The Duffing Equation, Nonlinear Oscillators and their Behavior* (Wiley, Chichester) 2011.
[13] Argyris J., Faust G., Haase M. and Friedrich R., *An Exploration of Dynamical Systems and Chaos*, 2nd edition (Springer, New York) 2015.
[14] Strogatz S., *Nonlinear Dynamics and Chaos with Applications to Physics, Biology, Chemistry, and Engineering*, 2nd edition (Westview Press, Boulder) 2015.
[15] Freire J. G., Gallas M. R. and Gallas J. A. C., *Eur. Phys. J. ST*, **226** (2017) 1987.
[16] Ueda Y., *The Road to Chaos* (Aerial Press, Santa Cruz) 1992, freely available on the internet from `http://hdl.handle.net/2433/71101`.
[17] Sack A., Freire J. G., Lindberg E., Pöschel T. and Gallas J. A. C., *Sci. Rep.*, **3** (2013) 3350 and references therein.
[18] Leyton V., Thorwart M. and Peano V., *Phys. Rev. B*, **84** (2011) 134501.
[19] Parlitz U. and Lauterborn W., *Phys. Lett. A*, **107** (1985) 351.
[20] Paar V. and Paivin N., *Phys. Rev. E*, **57** (1998) 1544.
[21] Freire J. G. and Gallas J. A. C., *Phys. Chem. Chem. Phys.*, **13** (2011) 12191.
[22] Gallas J. A. C., *Adv. At. Mol. Opt. Phys.*, **65** (2016) 127.
[23] Freire J. G., Cabeza C., Marti A., Pöschel T. and Gallas J. A. C., *Sci. Rep.*, **3** (2013) 1958.
[24] Freire J. G., Cabeza C., Marti A., Pöschel T. and Gallas J. A. C., *Eur. Phys. J. ST*, **223** (2014) 2857.
[25] Singla T., Sinha T. and Parmananda P., *Chaos, Solitons Fractals*, **75** (2015) 212.
[26] Shaw P. K., Janaki M. S., Iyengar A. N. S., Singla T. and Parmananda P., *Chaos, Solitons Fractals*, **78** (2015) 256.
[27] Rao X. B., Chu Y. D., Xu L., Chang Y. X. and Zhang J. G., *Commun. Nonlinear Sci. Numer. Simul.*, **50** (2017) 330.
[28] Tomita K., Kai T. and Hikami F., *Prog. Theor. Phys.*, **57** (1977) 1159.
[29] Knudsen C., Sturis J. and Thomsen J. S., *Phys. Rev. A*, **44** (1991) 3503.
[30] Tomita K., *Phys. Rep.*, **86** (1982) 113.
[31] Hao B. L., *Elementary Symbolic Dynamics and Chaos in Dissipative Dynamical Systems* (World Scientific, Singapore) 1989.
[32] Hao B.-L. and Zheng W.-M., *Applied Symbolic Dynamics and Chaos* (World Scientific, Singapore) 1989.
[33] Hao B. and Zheng W., *Applied Symbolic Dynamics and Chaos*, 2nd revised edition (Peking University Press, Beijing) 2014, ISBN 978-7-301-24756-3.
[34] Gallas J. A. C., *Mod. Phys. Lett. B*, **29** (2015) 1530018 and references therein.
[35] Lorenz E. N., *J. Atmos. Sci.*, **49** (1992) 2449.